Article ID: 1003－6326(2004)03－0525－05

Equal channel angular deformation process and its neuro-simulation for fine-grained magnesium alloy①

LUO Peng(罗 蓬)[1], HU Qiao-dan(胡侨丹)[2], WU Xiao-lin[3], XIA Ke-nong[3]
(1. School of Mechanical Engineering and Automation,
Guizhou University of Technology, Guiyang 550003, China;
2. School of Manufacturing Science and Engineering,
Sichuan University, Chengdu 610065, China;
3. Materials Group, Department of Mechanical and Manufacturing Engineering,
University of Melbourne, VIC 3010, Australia)

Abstract: Fine-grained structure of as-cast magnesium AM60 alloy was obtained by means of equal channel angular deformation(ECAD) technique. Through analyzing the relationship between the load and the displacement under different working conditions, it is demonstrated that employment of back-pressure, multi-passages of deformation, and speed of deformation are the main factors representing ECAD working condition. As for ECAD process, a network composed of non-linear neuro-element based on error back-propagation learning algorithm is launched to set up a processing mapping module for dynamic forecasting of load summit under different working conditions. The experimental results show that back-pressure, multi-passages and deforming speed have strong correlation with ECAD processing characteristics. On the metallographs of AM60 alloy after multi-passes ECAD, a morphology that inter-metallic compound $Mg_{17}Al_{12}$ precipites on magnesium matrix without discrepancy, which evolves from coarse casting ingot microstructure, is observed. And the grains are refined significantly under accumulated severe shear strain. The study demonstrates feasibility of ECAD by using as-cast magnesium alloy directly, and launches an intelligent neuro-simulation module for quantitative analysis of its process.

Key words: magnesium alloy; ECAD; fine-grained structure; neuro-simulation
CLC number: TG 146.2; TG 376.2 **Document code:** A

1 INTRODUCTION

Equal Channel Angular Deformation(ECAD) is a novel and promising technique of fine-grained structure nonferrous alloys by means of accumulated severe shear strain[1, 2]. With ECAD, submicrometer-grained structure can be produced[1]. Up to date, some ECAD works have been taken referring to aluminum alloys[2-5]. In China, a number of studies have been reported mainly concerning pure aluminum and copper single crystal[6-11], which concentrated on evolution of microstructure, shear strain characteristics, and finite element simulation of deformation process. Meanwhile, ECAD work for magnesium alloys, which are more liable to produce cracks under shear strain due to their HCP structure, is still in the experimental study stage[12-15]. Although it was reported that after ECAD, the microstructure refinement of pure Mg, Mg-0.9%Al and dilute Mg-0.6% Zr alloy were achieved[16, 17], and low temperature super-plastic forming capability using high strain rate for magnesium AZ91 alloy could be obtained[18], up to now, few works are taken with ECAD for magnesium alloys.

This work applied ECAD technique to as-cast magnesium AM60 ingot, whose microstructure was too coarse to be pre-extruded for ECAD. Through ECAD tests, the effects of working conditions, e.g. the number of multi-passages, backpressure, and speed of deformation, on the process characteristics and evolution of microstructure under accumulated severe shear strain, were studied. In addition, in order to launch a way of CAD/CAE for potential industrial practice, an intelligent neuro-simulation module based on the error back-propagation neural network was established to provide a quantitative mapping analysis for dynamic forecasting of load summit during the magnesium ECAD under different working conditions. Under the MATLAB environment, the error back-propagation network uses an adaptive learning rate-momentum improved algorithm based on gradient-decent updating mechanism to simulate any kind

① **Foundation item:** Project (21852035) supported by the China Scholarship Council and the Australia Research Council
Received date: 2003－07－11; **Accepted date:** 2004－02－01
Correspondence: LUO Peng; Tel: +86-851-4730132; E-mail: luopeng_gut@hotmail.com

of non-linear mapping with arbitrary precision[19]. Thus, it is an agile and effective tool for intelligent modelling of ECAD process.

2 ECAD PROCESS FOR MAGNESIUM ALLOY

An ECAD die having a channel rectangular cross-sectional area of 9.1 mm × 9.1 mm and with an intersecting angle of 90° between the two parts of the channel, was made, as shown in Fig. 1. Billets in magnesium AM60 alloy were cut in size of 8 mm × 8 mm × 50 mm from casting ingots, due to the requirement that certain room should be left to graphite paper wrapped outside of the billet as lubricant. The tests were taken on Instron-8501 machine with hydraulic backpressure mechanism helpful to enhance the ECAD process stability. The die was heated by a heating element blanket. The temperatures for tests were continuously monitored within (573 ±1) K, by using a thermocouple inserted in a hole drilled into the die to a point within 4 mm of the channel wall at the initial point of deformation.

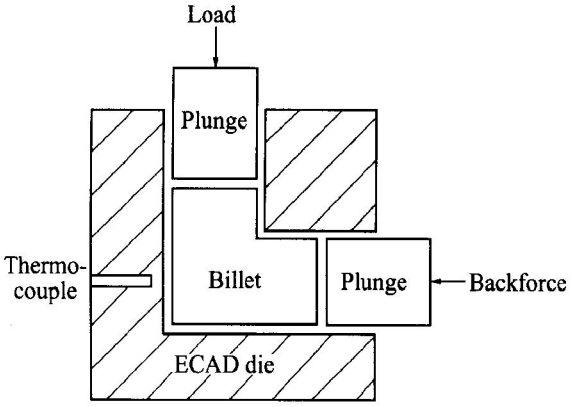

Fig. 1 Schematic diagram of ECAD die

Generally, after one passage, for the ECAD the shear strain is[20]

$$\gamma = 2\mathrm{ctg}\frac{\varphi}{2} \quad (1)$$

where φ is the angle of intersection of the two parts of channel. In the case of $\varphi = 90°$, as shown in Fig. 1, the shear strain produced by single-passage ECAD is $\gamma = 2$. Further more, in the ECAD, the billets undergo severe shear strain but retain the same cross-sectional geometry so that it is possible to repeat the deformations for multi-passages. In this case, the same shear strain is accumulated in each passage. Therefore, after N passages of ECAD, the total equivalent strain is represented[20, 21]:

$$\varepsilon_e = \frac{\gamma N}{\sqrt{3}} = \frac{2N}{\sqrt{3}}\mathrm{ctg}\frac{\varphi}{2} \quad (2)$$

In the case of $\varphi = 90°$, the total equivalent strain ε_e becomes

$$\varepsilon_e = 1.1547N \quad (3)$$

Thus, the strain produced by ECAD can be estimated from Eqn. (3) for any number of passages.

On the Instron machine, with different back-pressure, number of ECAD passages and speed of deformation, the ECAD testing results were obtained in the form of a series of load versus displacement curves, whose data were recorded by a data-logger from a sensor, as shown in Fig. 2.

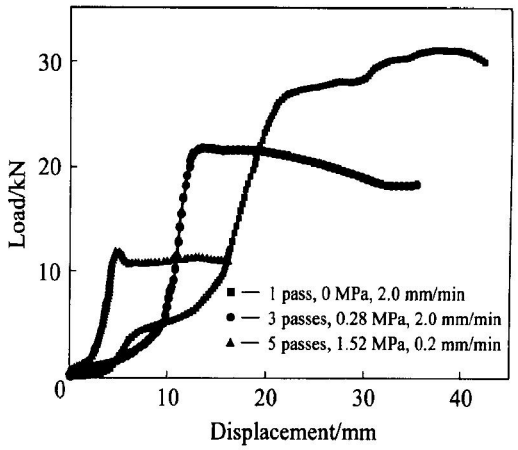

Fig. 2 Load versus displacement in ECAD of magnesium alloy

From Fig. 2, it is found that with employment of the back-pressure, the summit of the load is decreased. That is due to the fact that the back-pressure maintains the integrality of the graphite paper layer. Thus, the friction between the deformed billet and channel can be decreased significantly. Simultaneously, the back-pressure combined with low deforming speed was beneficial to stability of deformation process, which made the falling of the load summit as well. That can be testified by the case of passage number 5, back-pressure of 1.52 MPa with low deforming speed of 0.2 mm/min, where the slope of load versus displacement curve is nearly equal to zero during the normal stage of deformation.

Fig. 3 shows the microstructures of magnesium AM60 alloy after cast or after five ECAD passages.

Fig. 3 indicates that after multi-passage of ECAD, the microstructure of magnesium AM60 alloy evolves from coarse as-cast crystal to refined one with inter-metallic compound $Mg_{17}Al_{12}$ precipitating on magnesium matrix without discrepancy.

3 NEURO-SIMULATION OF ECAD PROCESS

In this work, Neuro-simulation of ECAD process of magnesium alloy refers to establishing a process mapping module for dynamic forecasting of load summit F_{max} under different working conditions repre-

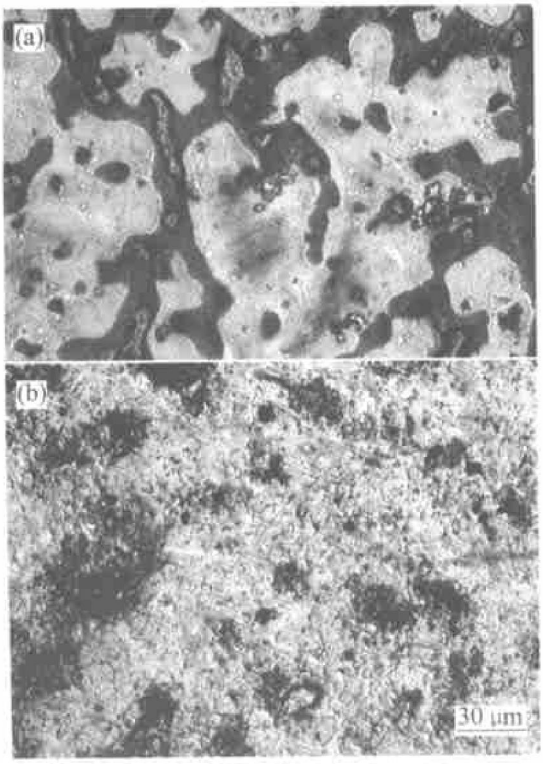

Fig. 3 Microstructures of magnesium AM60 alloy
(a) —As-cast; (b) —After five ECAD passages

sented by the number of ECAD passages N, deforming speed v, and back-pressure summit p_{max}. On the panel of Instron machine, the deforming speed can be set according to a series of options. And the back-pressure summit adjustments can be achieved through hydraulic valve of back-force mechanism.

3.1 Mathematical model of neuro-simulation

A sample input-output pair $(\boldsymbol{X}^{(k)}, \boldsymbol{d}^{(k)})$, $k = 1, 2, \cdots, p$, where $\boldsymbol{X}^{(k)} = [x_2^{(k)}, \cdots, x_j^{(k)}, \cdots, x_m^{(k)}]^T$ and $\boldsymbol{d}^{(k)} = [d_1^{(k)}, \cdots, d_i^{(k)}, \cdots, d_n^{(k)}]^T$, is given. A three-layer BP network is shown in Fig. 4, whose input layer has m neuro-elements, hidden layer has l elements, and output layer has n elements respectively. Given an input pattern $\boldsymbol{X}^{(k)}$, a neuro-element q in the hidden layer receives a net input:

$$n_q^{(k)} = \sum_{j=1}^{m} v_{q,i} \cdot x_j^{(k)} \tag{4}$$

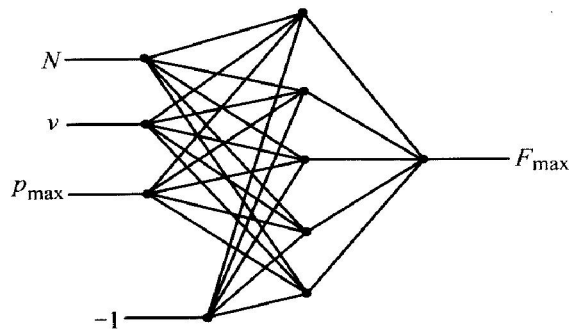

Fig. 4 Structure of neural network

where $v_{q,j}$ is a connective weight between neuro-element q in the hidden layer and element j in the input layer.

This net input produces an output:

$$z_q^{(k)} = f(n_q^{(k)}) \tag{5}$$

where $f(\cdot)$ is sigmoid activation function of a neuro-element in the form of

$$f(x) = \frac{1}{1 + \exp(-x)} \tag{6}$$

The net input for a neuro-element i in the output layer is then

$$n_i^{(k)} = \sum_{q=1}^{l} w_{i,q} z_q^{(k)} = \sum_{q=1}^{l} w_{i,q} f(n_q^{(k)}) \tag{7}$$

where $w_{i,q}$ is a connective weight between neuro-element i in the output layer and element q in the hidden layer, and the net input produces an output of

$$y_i^{(k)} = f(n_i^{(k)}) \tag{8}$$

Hence, the error signals $d_i^{(k)} - y_i^{(k)}$ is produced to define a sum-squared error (SSE) cost function:

$$E_k = \frac{1}{2} \sum_{i=1}^{n} (d_i^{(k)} - y_i^{(k)})^2 \tag{9}$$

Then according to gradient-descent algorithm[22], the connective weights in the hidden-to-output layer could be updated by

$$\Delta w_{i,q} = -\eta \frac{\partial E_k}{\partial w_{i,q}} \tag{10}$$

where η is the learning rate. Using Eqns. (6)~(9) and the chain rule for $\partial E_k / \partial w_{i,q}$, the updating of $w_{i,q}$ can be represented by

$$\begin{aligned} \Delta w_{i,q} &= -\eta \frac{\partial E_k}{\partial y_i^{(k)}} \frac{\partial y_i^{(k)}}{\partial n_i^{(k)}} \frac{\partial n_i^{(k)}}{\partial w_{i,q}} \\ &= \eta (d_i^{(k)} - y_i^{(k)}) z_q^{(k)} f'(n_i^{(k)}) \end{aligned} \tag{11}$$

Similarly, the weight updating on the input-to-hidden connections, can be expressed as

$$\begin{aligned} \Delta v_{q,i} = \eta x_j^{(k)} f'(n_q^{(k)}) \sum_{i=1}^{n} [(d_i^{(k)} - y_i^{(k)}) \cdot \\ w_{i,q} f'(n_i^{(k)})] \end{aligned} \tag{12}$$

Eqns. (11) and (12) mean a normal BP algorithm. In practice, a momentum term is frequently added to ensure a larger learning rate (for rapid convergence of network) without divergent oscillations occurring during network training procedure. At the same time, momentum term decreases network's sensitivity. That helps the network to avoid getting stuck in local minima which would prevent the network from finding a lower error solution[22]. Thus, Eqns. (11) and (12) become

$$\Delta w_{i,q}(t) = -\eta \frac{\partial E_k}{\partial w_{i,q}} + \alpha \Delta w_{i,q}(t-1) \tag{13}$$

$$\Delta v_{q,i}(t) = -\eta \frac{\partial E_k}{\partial v_{q,i}} + \alpha \Delta v_{q,i}(t-1) \tag{14}$$

where $\alpha \in [0, 1]$ is a momentum parameter, and t is the iteration epoch during network training.

In addition, since the best value of learning rate at the beginning of training may not be good in later training process, a more efficient approach is adopted to an adaptive learning rate[23]. Firstly, whether a weight updating has decreased the cost function is checked. If it has, increase the learning rate, that is,

if $\Delta E_k(t) = E_k(t) - E_k(t-1) < 0$,

then $\eta(t+1) = \eta(t) + \lambda\eta(t)$ (15)

where λ is the learning rate increase multiplier.

At the same time,

if $\Delta E_k(t) = E_k(t) - E_k(t-1) \geqslant 0$,

then $\eta(t+1) = \eta(t) - \beta\eta(t)$ (16)

where β is the learning rate decrease multiplier.

3.2 Neuro-simulation for ECAD process of magnesium alloy

Applying the neuro-simulation model discussed above to ECAD process of magnesium alloy, where $m = 4$; $l = 5$; and $n = 1$. $\boldsymbol{X}^{(k)} = [N^{(k)}, v^{(k)}, p_{\max}^{(k)}, -1]^{\mathrm{T}}$; $\boldsymbol{d}^{(k)} = [F_{\max}^{(k)}]^{\mathrm{T}}$, $k = 1, 2, \cdots, p$. For convenience of expression, the thresholds of all the neuro-elements on hidden and output layer are treated as the weights connected with an input permanently equal to -1, as shown in Fig. 4. The selection of number for neuro-element on hidden layer is made intuitively[24], only if the number could ensure the network simulate a certain mapping with sufficient precision.

According to the ECAD testing results shown in Fig. 2, sample input-output pairs ($\boldsymbol{X}^{(k)}$, $\boldsymbol{d}^{(k)}$) used to train the network are provided by intelligent reasoning rules with If-Then format, e.g., {For $k = 1$, If $N^{(1)} = 1$ And $v^{(1)} = 0.2$ mm/min And $p_{\max}^{(1)} = 0.40$ MPa, Then $F_{\max}^{(1)} = 1.60 \times 10^4$ N}. From the testing data, forty sample pairs were adopted for training ($p = 40$).

With neural network toolbox of MATLAB environment, the simulation was realized. In the toolbox, the training of an error back-propagation network with adaptive learning rate-momentum algorithm is implemented by function trainbpx[19].

During the training, the estimated error goal was set as 0.01, the momentum parameter was $\alpha = 0.95$, the initial learning rate η was set as 0.000 1, the learning rate increase multiplier was $\lambda = 1.05$, and the learning rate decrease multiplier was $\beta = 0.7$. After training epochs of 1321, the network made convergence to SSE(1321) = 0.009 9, less than 0.01. As the results, sum-squared error (SSE) and adaptive learning rate(ALR) versus iteration epoch relations are given in Fig. 5.

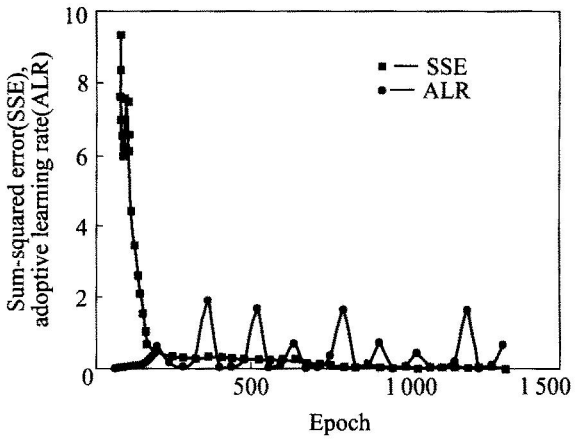

Fig. 5 SSE and ALR versus epoch

Table 1 lists the connective weights and thresholds distribution when training is converged. Hence, the neural network can be used to forecast the load summit $F_{\max}$ under different ECAD working conditions. Table 2 shows the forecasting load summits $F_{\max 1}$, by neuro-simulation, compared with the actual values of $F_{\max 2}$, measured by the sensor during the ECAD tests.

Table 2 shows that the forecasting precisions are over 97%. The ECAD load summits forecasted by neural network fit the actual measurements quite well. With the progress of the experimental plan, new testing data are produced. Thus the sample pairs for training of neural network can be augmented. That perfects the mapping capability of neuro-simulation gradually. Therefore, the

Table 1 Connective weights and thresholds of neural network

Hidden layer, q	Hidden layer threshold	Input layer, j			Output laryer, i	Output layer threshold
		1	2	3		
1	− 0.283 7	0.692 8	0.867 3	− 0.329 6	0.018 1	
2	0.542 2	− 0.626 2	− 0.042 7	− 2.776 0	1.911 1	
3	1.332 3	0.824 3	0.906 0	0.750 7	− 0.376 5	− 0.1793
4	− 1.116 2	0.479 1	0.734 8	− 1.998 5	2.551 7	
5	0.612 6	1.642 4	− 0.811 9	− 0.877 7	1.325 1	

Table 2 Forecasting ECAD load summits compared with actual testing results

N	v/(mm·min^{-1})	p_{max}/MPa	F_{max1}/kN	F_{max2}/kN	Error/%
1	5.0	0.00	28.992	29.0	0.028
1	2.0	0.00	29.854	30.0	0.49
1	0.2	0.40	16.002	16.0	0.02
1	2.0	0.28	22.377	22.0	1.68
2	2.0	0.53	22.172	22.8	2.754
3	2.0	0.78	22.118	21.5	2.794
4	2.0	1.20	19.757	20.0	1.215
5	0.2	1.52	12.127	12.1	0.23

F max1—Forecasting load summit;
F max2—Actual load summit;

forecasting module is established dynamically. It is characterized by a capability of self-updating and perfecting.

REFERENCES

[1] Furukawa M, Horita Z, Nemoto M, et al. Review processing of metals by equal-channel angular pressing[J]. J Mater Sci, 2001, 36: 2835-2843.

[2] Horita Z, Fujinami T, Langdon T G. The potential for scaling ECAP: effect of sample size on grain refinement and mechanical properties[J]. Mater Sci Eng, 2001, A318: 34-41.

[3] Zhu Y T, Lowe T C. Observations and issues on mechanisms of grain refinement during ECAP process[J]. Mater Sci Eng, 2000, A291: 46-53.

[4] Gholinia A, Prangnell P B, Markushev M V. The effect of strain on the development of deformation structures in severely deformed aluminum alloys processed by ECAE[J]. Acta Mater, 2000, 48: 1841-1851.

[5] LIU Ying, LI Yuan-yuan, ZHANG Da-tong. Development of equal channel angular pressing on metals[J]. Materials Science & Engineering, 2002, 20(4): 613-617, 486. (in Chinese)

[6] ZHAO Ren-xian, ZHANG Jian, WANG Zhi-qi, et al. Microstructure of pure aluminum under equal channel angular pressing[J]. Nonferrous Metals, 2002, 54(2): 8-11. (in Chinese)

[7] LI Yong-xia, ZHANG Yong-gang, CHEN Chang-qi. Effect of equal channel angular pressing on microstructure and mechanical properties of high pure aluminum[J]. Journal of Aeronautical Materials, 2001, 21(3): 33-38. (in Chinese)

[8] LI Qiang. Microstructure Evolution of High Pure Aluminum and Alloys by Equal Channel Angular Extrusion[D]. Shenyang: Institute of Metal Research, The Chinese Academy of Sciences, 2000. (in Chinese)

[9] LIU Yong, TANG Zhi-hong, ZHOU Ke-chao, et al. Equal channel angular pressing(ECAP) process of pure Al(Ⅰ)—Microstructure evolution[J]. The Chinese Journal of Nonferrous Metals, 2003, 13(1): 21-26. (in Chinese)

[10] LIU Yong, TANG Zhi-hong, ZHOU Ke-chao, et al. Equal channel angular pressing (ECAP) process of pure Al(Ⅱ)—Simulation of deformation behavior[J]. The Chinese Journal of Nonferrous Metals, 2003, 13(2): 294-299. (in Chinese)

[11] WU Shi-ding, LI Qiang, JIANG Chuan-bin, et al. Shear characteristics of copper single crystal during equal channel angular extrusion[J]. Acta Met Sinica, 2000, 36(6): 602-607. (in Chinese)

[12] LIU Zheng, ZHANG Kui, ZENG Xiao-qin. Fundamental Theory of Magnesium-Matrix Light Weighted Alloys Application[M]. Beijing: China Machine Press, 2002. (in Chinese)

[13] YU Kun, LI Wen-xian, WANG Ri-chu, et al. Research, development and application of wrought magnesium alloys[J]. The Chinese Journal of Nonferrous Metals, 2003, 13(2): 277-288. (in Chinese)

[14] LE Qi-chi, ZHANG Xin-jian, CUI Jian-zhong. Magnesium alloys: current status of their forming processes and applications[J]. Materials Review, 2002, 16(12): 12-15. (in Chinese)

[15] ZHANG Shi-jun, LI Wen-xian, YU Kun, et al. The grain refinement process of magnesium alloys[J]. Foundry, 2001, 50(7): 373-375. (in Chinese)

[16] Horita Z, Matsubara K, Makii K, et al. A two-step processing route for achieving a super-plastic forming capability in dilute magnesium alloys[J]. Scripta Mater, 2002, 47: 255-260.

[17] Yamashita A, Horita Z, Langdon T G. Improving the mechanical properties of magnesium and a magnesium alloy through severe plastic deformation[J]. Mater Sci Eng, 2001, A300: 142-147.

[18] Mabuchi M, Iwasaki H, Yanase K, et al. Low temperature superplasticity in an AZ91 magnesium alloy processed by ECAE[J]. Scripta Mater, 1997, 36(6): 681-686.

[19] Demuth H, Beale M. Neural Network Toolbox for Use with MATLAB: User's Guide[M]. The MathWorks Inc, 1993.

[20] Iwahashi Y, Wang J, Horita Z, et al. Principle of equal-channel angular pressing for the processing of ultra-fine grained materials[J]. Scripta Mater, 1996, 35(2): 143-146.

[21] Xia K, Wang J. Shear, principal, and equivalent strains in equal-channel angular deformation[J]. Metall and Mater Trans A, 2001, 32A: 2639-2647.

[22] Papalambros P Y, Wilde D J. Principles of Optimal Design: Modeling and Computation[M]. Cambridge: Cambridge University Press, 2000.

[23] Lin C T, Lee C S G. Neural Fuzzy Systems: A Neuro-fuzzy Synergism to Intelligent System[M]. Upper Saddle River, NJ: Prentice-Hall PTR, 1996.

[24] YAN Ping-fan, ZHANG Chang-shui. Artificial Neural Network and Evolutionary Algorithm[M]. Beijing: Tsinghua University Press, 2000. (in Chinese)

(Edited by YANG Bing)